*Chinese Journal of Polymer Science Vol. 34, No. 2, (2016), 164–173*

***Chinese Journal of Polymer Science***
© Chinese Chemical Society
Institute of Chemistry, CAS
Springer-Verlag Berlin Heidelberg 2016

# Enhanced Mechanics in Injection Molded Isotactic Polypropylene/Polypropylene Random Copolymer Blends *via* Introducing Network-like Crystal Structure

Bi-qiang Jin, Xin-peng Li, Ming Jin, Da-shan Mi, Fei-fei Wang, Chao Xia and Jie Zhang*
*State Key Laboratory of Polymer Materials Engineering, College of Polymer Science and Engineering, Sichuan University, Chengdu 610065, China*

**Abstract** The crystallization behavior, rheological behavior, mechanical properties and microstructures of injection molded isotactic polypropylene (*i*PP), polypropylene random copolymer (*co*-PP) and *i*PP/*co*-PP blends were investigated. Differential scanning calorimetry (DSC) and dynamic rheological analysis illustrated that *i*PP and *co*-PP were compatible in the blends and *co*-PP uniformly dispersed in the *i*PP phase. Polarizing optical microscope (POM) was adopted to observe the crystal size and morphology evolution. The results of mechanical properties and scanning electron microscopy (SEM) indicated that the crystal size of *i*PP in *i*PP/*co*-PP blends (10 wt% *co*-PP + 90 wt% *i*PP and 30 wt% *co*-PP + 70 wt% *i*PP) radically decreased after the incorporation of *co*-PP. During crystallization, the molecular chain segments of *co*-PP could penetrate *i*PP spherulites and form a network-like crystalline structure. The network-like crystal structure could effectively transmit stress and consume more energy to overcome intermolecular forces to resist stretching. In this way, the strength would improve to a certain degree. The impact fracture mechanism of *i*PP/*co*-PP blends is quasi ductile fracture by multiple crazes. Our work discovered that the blends containing 10 wt% and 30 wt% of *co*-PP exhibited prominent toughness and reinforcement.

**Keywords:** Network-like; Morphology; Toughness; Polypropylene random copolymer.

## INTRODUCTION

Since the industrialization started in 1957, the constant improvement of polypropylene catalyst technology and manufacturing technique have reduced the production costs of polypropylene and greatly improved its performance. The consumption of polypropylene became relatively high among general resins. Polypropylene could be categorized into polypropylene homopolymer (PPH), or isotactic polypropylene (*i*PP)[1–3], polypropylene random copolymer (*co*-PP)[4, 5], impact polypropylene copolymer (IPC), or rather polypropylene block copolymer (PPB)[6–8] and polypropylene catalloy (PP-c)[9, 10], *etc*.

With relatively comprehensive performance including easy processing, strong resistance to thermal deformation and high strength, *i*PP became the most widely used commercialized plastic raw material. Under conventional injection molding conditions, *i*PP, however, generates large-sized $\alpha$-spherulites. With such crystalline structure, *i*PP exhibits relatively low impact strength, especially at low temperatures its toughness is quite poor. Its low impact strength seriously constrained the application of *i*PP. Therefore, the academic community has paid wide attention to improve its toughness and conducted many researches in this regard[11–14].

*co*-PP is the copolymerized product of propylene and ethylene. A small quantity of ethylene (a content of 1 wt%–5 wt%) is added into propylene to produce an easily processing copolymer with a low melting point and comparatively high transparency during polymerization. The low-temperature impact property of *co*-PP is

* Corresponding author: Jie Zhang (张杰), E-mail: zhangjie@scu.edu.cn
Received August 5, 2015; Revised September 21, 2015; Accepted October 23, 2015
doi: 10.1007/s10118-016-1747-y

markedly improved compared with that of *i*PP. Meanwhile, it maintains other eminent properties of polypropylene[15].

In view of the compatibility of *i*PP and *co*-PP, *co*-PP modified *i*PP may optimize the performance of *i*PP/*co*-PP blends. So far, studies on the modification of *i*PP/*co*-PP blends have been rarely conducted. In this paper the crystalline behavior, rheological behavior, mechanical properties and microstructures of *i*PP, *co*-PP and *i*PP/*co*-PP blends were investigated with the aim of providing a more economical and practical method for the modification of *i*PP.

## EXPERIMENTAL

### *Materials*

The isotactic polypropylene (*i*PP, trademarked as T30S) was supplied by Lanzhou Petrochemical Company, China, with a melt flow index (MFI) of 2.6 g/10min (230 °C/2.16 kg) and a density of 0.91 g/cm$^3$, respectively. The polypropylene random copolymer (*co*-PP), RP2400, was purchased from YUHWA Korea petrochemical Ind. Co., Ltd, with a $M_w = 5.8 \times 10^4$ g/mol and a melt flow rate (MFR) of 0.25 g/10min measured at 230 °C under 2.16 kg. The molar percentage of ethylene component was about 4%.

### *Sample Preparation*

The *i*PP and *co*-PP were melted and mixed by a twin-screw extruder with a temperature profile of 170, 180, 200, 200, 190 °C from hopper to die. After drying at 80 °C for 12 h, the pelletized granules were subsequently injection-molded into standard specimens, conducted on a PS40E5ASE injection molding machine with a barrel temperature of 200 °C, mold temperature of 60 °C and injection pressure of 34 MPa, respectively. Seven series of samples were prepared for this research. The blends are denoted as C10, C30, C50, C70 and C90, where the numbers indicate the percent weight content of *co*-PP in the blends. For example, the blends of 70 wt% *co*-PP + 30 wt% *i*PP are named as C70.

### *POM Observation*

In order to investigate the size of $\alpha$-spherulites and morphology evolution, POM observation was used. The thin slices used to observe the crystal size were cut by means of a microtome, and the films used for variable-temperature observation were prepared by squeezing *i*PP melt between two cover glasses. Polarized light microscopy observations were performed with a DX-1 (Jiang Xi Phoenix Optical Co., China.) microscope with 45° and 90° cross-polarized light connected with a Nikon 500D digital camera and a hot stage (HB-2002, Skyray Instrument, China).

### *DSC Measurements*

A computerized Perkin-Elmer differential scanning calorimeter (Model CDR-4P, Shanghai Precision & Scientific Instrument Corporation, Shanghai, China) was used for DSC measurements. The weights of the specimens were about 6 mg. During the measurement, dried $N_2$ gas was purged at a constant flow rate. The heating rate was 10 K/min. The temperature readings and calorific measurements were calibrated by using standard indium.

### *WAXD Measurements*

The wide-angle X-ray diffraction experiments (WAXD) were conducted using a Philips X'Pert Pro diffractometer. The wavelength of the monochromated X-ray from CuK$\alpha$ radiation was 0.154 nm and projection mode was used. The scanning $2\theta$ range was from 10 to 40 degrees. The degree of crystallinity, $X_c$, can be also determined from the WAXD patterns based on the ratio of the integrated intensities under the crystalline peaks Ac to the integrated total intensities, $A = A_c + A_a$ in which $A_a$ is the integrated intensities under the amorphous halo.

$$X_c = \frac{A_c}{A_c + A_a} \times 100\% \quad (1)$$

### *Dynamic Rheology Measurements*

Dynamic rheology property was investigated by a rotational rheometer (Malvern Instruments, Bohlin Gemini 200). Steady shear measurement was performed at the shear rate of 0.01−100 $s^{-1}$ at 180 °C. The shear strain was kept at a constant of 2%.

### *Mechanical Property Tests*

A Shimadzu universal testing machine (Model RGT-10, Ruigerer Corporation, Shenzhen, China) was used for tensile testing at room temperature (23 °C) at a crosshead speed of 50 mm/min according to ASTM D638-03 standard. A VJ-40 (Chengde Experimental Factory, Hebei, China) impact machine was employed to do impact testing at room temperature (23 °C) according to ASTM D256-04 standard. A 1 mm V indentation was milled in the middle of the samples with the help of a milling machine (model XQZ-1, Minks Detection Equipment Co., Ltd., Xi'an, China).

### *Scanning Electron Microscopy (SEM)*

A Hitachi scanning microscope (Model S-450, Hitachi, Osaka, Japan) was used to investigate the impact fracture surfaces and the etched sample surfaces. The impact fracture surfaces were examined directly after impact property test, while the etched sample surfaces were treated by permanganic etches for observation as described by Bassett *et al*[16]. The etching samples were etched in a solution of $KMnO_4$-$H_2SO_4$-$HNO_3$-$H_3PO_4$ at a constant temperature of 30 °C for 24 h. The surfaces of all the samples were sputter-coated with a layer of gold to provide enhanced conductivity. Then the morphology was observed in a field emission SEM, operating at 20 kV.

## RESULTS AND DISCUSSION

### *Crystalline and Dynamic Rheology Behaviors*

Before exploring the variation of morphology after the addition of *co*-PP in *i*PP samples and its influence on the mechanical properties, it is reasonable to investigate the crystalline and rheology behaviors firstly.

Figure 1(a) represents the DSC melting curves of *i*PP, *co*-PP and *i*PP/*co*-PP blends. It can be clearly seen that only a single melting peak appears in the pure *co*-PP melting curve, with a melting point of 149.58 °C, about 18 K lower than that of pure *i*PP. This is mainly because a small number of vinyl monomers have been added to *co*-PP during polymerization and the ethylene is irregularly distributed in *co*-PP molecular chains, which lowered the crystallinity and melting point of *co*-PP[17]. The C70 and C90 have two melting endothermic peaks, which are around 148 °C and 156 °C, respectively. They stand for *co*-PP and *i*PP respectively. The samples dominated by *co*-PP show double melting peaks, indicating different levels of crystalline structures are formed. With the increase of *i*PP content, the melting point of *i*PP/*co*-PP blends rises gradually. When the content of *i*PP reaches 50 wt%, the blends show only one melting peak with the value of 160.22 °C, 10.64 K higher than that of pure *co*-PP, which demonstrates that *co*-PP is compatible with *i*PP and only one crystalline modification is formed in the blends, namely, $\alpha$-crystals. The thermal stability of the blends also increased comparatively.

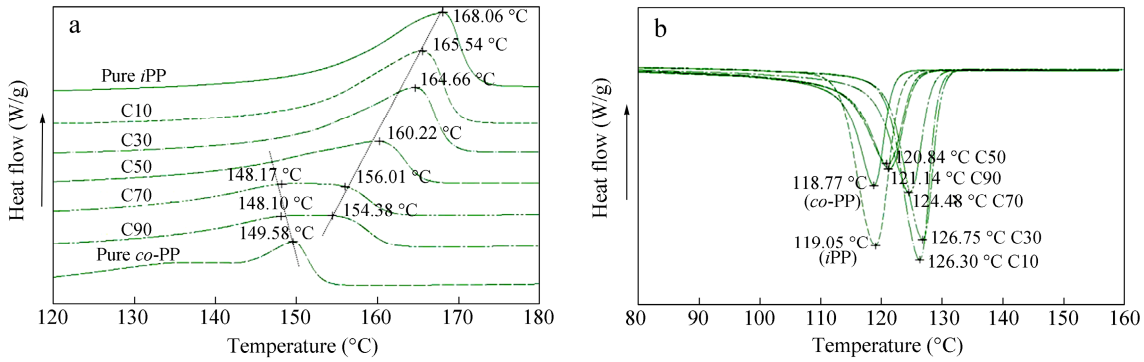



**Fig. 1** DSC (a) melting curves and (b) crystallization curves of *i*PP, *co*-PP and *i*PP with different contents of *co*-PP

The DSC crystallization curves are shown in Fig. 1(b). Both pure *co*-PP and *i*PP exhibit relatively low crystallization temperature ($T_c$)-119 °C, but the $T_c$ of *co*-PP/*i*PP blends is higher than that of pure samples. Interestingly, *co*-PP/*i*PP blends with lower *co*-PP contents (C10 and C30) show much higher $T_c$. When *co*-PP content is 10 wt%, the crystallization temperature increases by 7.25 K compared with that of pure *i*PP. The reason might be that *co*-PP could act as heterogeneous nucleating agent to induce stable nucleus under a low degree of supercooling, making *i*PP crystallize at higher temperatures, thus raise the crystallization temperature of the blends.

Figure 2 presents the WAXD curves of *i*PP, *co*-PP and *i*PP/*co*-PP blends. The diffraction peaks of *i*PP and *i*PP/*co*-PP blends appear at 14.1°, 16.9°, 18.5°, 21.3° and 22.0°. The corresponding lattice planes are respectively $\alpha$(110), $\alpha$(040), $\alpha$(130), $\alpha$(111) and $\alpha$(041) and all of them are monoclinic crystals ($\alpha$-crystals) of *i*PP. This illustrates that *i*PP/*co*-PP blends generate only $\alpha$-modification. It is consistent with the results of the DSC melting curves.

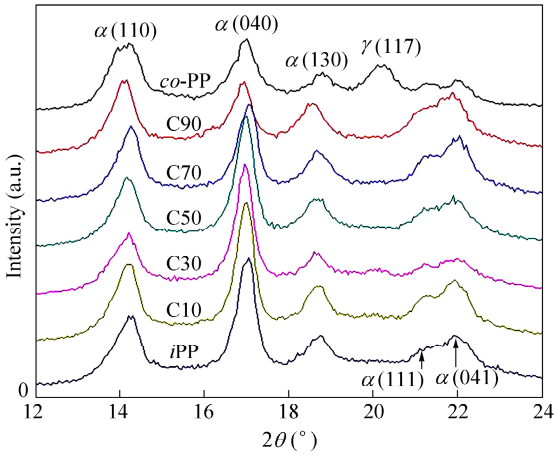



**Fig. 2** WAXD curves of *i*PP, *co*-PP and *i*PP/*co*-PP blends

But for *co*-PP, the characteristic peak of $\gamma$ crystal ($\gamma$(117)) emerges at $2\theta = 20.2°$. The explanation might be found in the specific characteristics of *co*-PP chains, where a uniform concentration of defects (stereo- and regioerrors) is present throughout the different macromolecules. It has been reported[18–20] that the development of the $\gamma$ phase is favored by interrupting isotactic segments, so the maximum content of $\gamma$ modification formed is directly proportional to the concentration of those defects, *i.e.*, inversely proportional to the average length of isotactic sequences. These results suggest that a small quantity of *i*PP can provide enough isotactic segments in *i*PP/*co*-PP blends that inhibit *co*-PP to form $\gamma$-crystals and only monotonous $\alpha$-crystals occur.

Table 1 shows the degree of crystallinity obtained from both the DSC and WAXD analyses. It is noted that the values of the crystallinity obtained from the WAXD analysis are relatively higher than those from DSC measurement. The crystallinity of C10 and C30 are almost the same as pure *i*PP, which indicates that a small amount of *co*-PP cannot change the crystallinity significantly. But when more *co*-PP are added, the crystallization degree decreases with the increment of *co*-PP. Large contents of low crystallinity *co*-PP in C50, C70 and C90 result in the decrease of crystallization degree. So the crystallization degree is greatly influenced by the content of *co*-PP.

**Table 1.** Crystallinity of all samples obtained from the DSC and WAXD analyses

| Samples | *i*PP | C10 | C30 | C50 | C70 | C90 | *co*-PP |
|---|---|---|---|---|---|---|---|
| WADX ($X_c$) | 0.62 | 0.63 | 0.62 | 0.60 | 0.56 | 0.54 | 0.48 |
| DSC ($X_c$) | 0.40 | 0.42 | 0.42 | 0.38 | 0.35 | 0.32 | 0.25 |

The dynamic rheology behaviors are depicted in Fig. 3, which records the variety of complex viscosity as a function of frequency. All samples exhibit non-Newtonian fluid behaviors (shear thinning) in the whole shear rate range. Pure *co*-PP and *i*PP show lower complex viscosities compared with those of *co*-PP/*i*PP blends. This may be because the molecular chain segments in pure samples having larger free volume can move more easily. But the *co*-PP/*i*PP blends exhibit higher complex viscosity than that of neat samples, which may result from the good compatibility of *co*-PP and *i*PP. It is in accordance with the DSC results. The entanglement of *co*-PP segments with *i*PP segments would decrease the free volume and weaken the locomotivity of chain segments, thus lead to the increase of the complex viscosity[21–23].

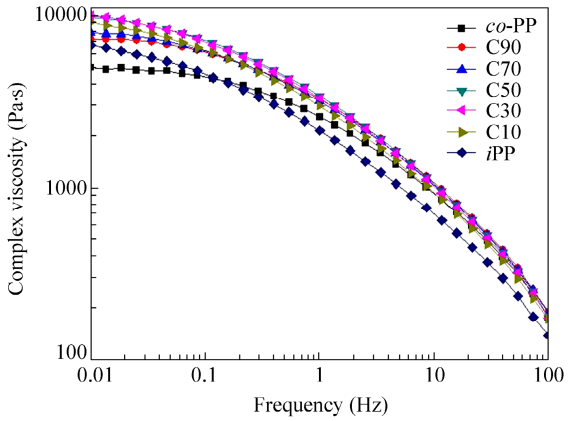



**Fig. 3** The complex viscosity as a function of frequency for *i*PP, *co*-PP and *i*PP/*co*-PP blends

***Mechanical Properties***

Figure 4 shows the impact strength and tensile strength of all the samples. The toughness of the samples generally increases with *co*-PP content. Surprisingly, when small amount of *co*-PP (10 wt%) is added, the impact strength of C10 (9.1 kJ/m$^2$) is nearly twice of that of pure *i*PP (4.6 kJ/m$^2$). The tensile strength of C10 sample has no decrease but a slight increase. With further increasing the content of *co*-PP, the impact strength of *co*-PP/*i*PP blends shows a stable increase whereas the tensile strength gradually decreases. It can be seen that the excellent mechanical properties are found in C10.

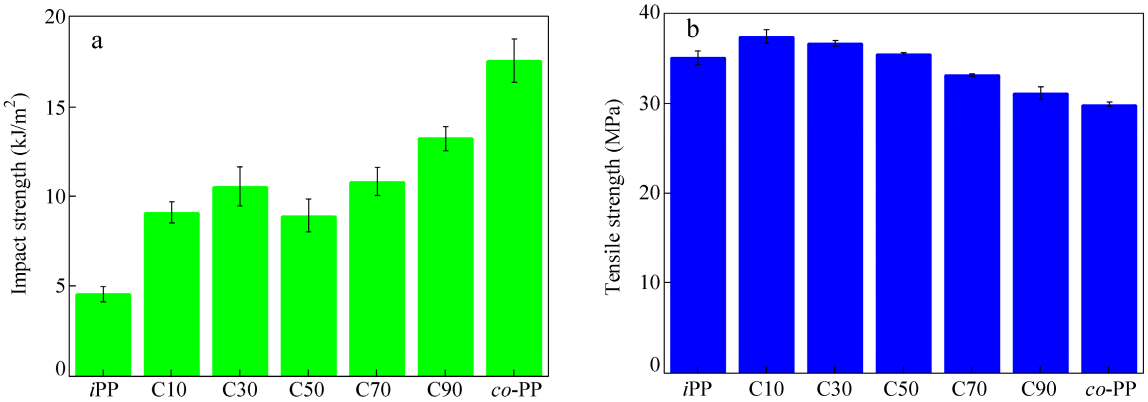



**Fig. 4** Mechanical properties of *i*PP, *co*-PP and *i*PP/*co*-PP blends: (a) impact strength and (b) tensile strength.

Researches on the aforementioned mechanical properties reveal that the incorporation of small amount of *co*-PP (10 wt% and 30 wt%) dramatically improve the mechanical properties of the blends in comparison with those of *i*PP. The addition of *co*-PP may change the inner morphological structure of *i*PP/*co*-PP blends. So a meticulous experiment (SEM) on morphological observation has been conducted.

***Morphology Observations***

Figure 5 reports the SEM of the impact-fractured surface of *i*PP, C10, C30 and *co*-PP. It can be seen that the fracture surface of pure *i*PP is relatively smooth, indicative of a brittle behavior. The results reveal that the cracks are induced and spread at an extremely rapid rate in the fracturing process, and the cracking is typical brittle fracture. The fracture here is caused by *i*PP crystalline morphology, which is monotonous crystalline form ($\alpha$-crystals) with large-sized $\alpha$-spherulites that limit the toughness. Although the fracture trigger region exhibits typical brittle fracture features, a few patch-shaped surfaces are discovered by closer observation. The patch-shaped surfaces, however, are seldom, so it is still brittle fracture.

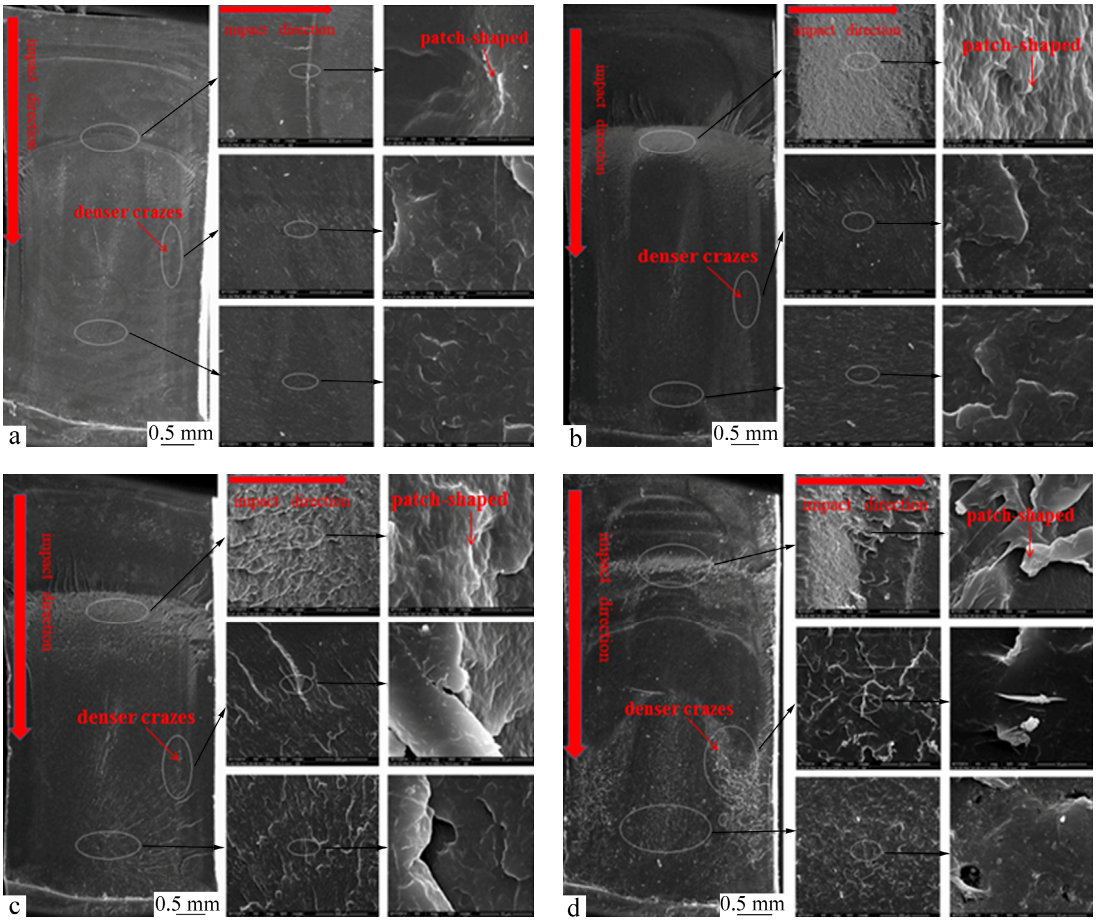



**Fig. 5** Impact-fractured surface morphology at different magnifications of (a) *i*PP (b) C10 (c) C30 and (d) *co*-PP

The impact-fractured surface of C10 and C30 is relatively rough, as shown in Figs. 5(b) and 5(c), which suggests that the incorporation of a small amount of *co*-PP can lead to ductile behavior. Compared with pure *i*PP, the corresponding regions of fracture are distinctly different. C10 and C30 samples have more patch-shaped surfaces in the fracture trigger zone than those of pure *i*PP. Meanwhile, some local plastic deformation microcells seem to be present on the surface of the patches. This demonstrates that, influenced by the impact effect, *co*-PP, as the stress concentration point, leads the surrounding *i*PP to generate denser crazes (namely, multiple crazes) and some shear zone. Thus the multiple crazes caused by *co*-PP increase energy consumption in *i*PP matrix during impact fracture process. As a result, *co*-PP plays a role as elastomer in the system. As Fig. 5(d) illustrates, pure *co*-PP shows the characteristics of ductile fracture, which is caused by the compositions and structures of *co*-PP[24–28].

Figure 6 and Figure 7 compare the inner crystal size and structures of the samples. Pure *i*PP has comparatively complete crystalline structure, clear-cut interfaces and large-sized spherulites about 20 μm, as shown in Figs. 6(a) and 7(a′). The addition of *co*-PP effectively refines spherulites in *i*PP/*co*-PP blends, which are presented in Figs. 6(b) and 6(c), and generates numerous well-distributed tiny spherulites about 8 μm (Figs. 7b′ and 7c′). It can be seen that *co*-PP is well-distributed in *i*PP matrix. The addition of *co*-PP can maintain the crystalline morphology of *i*PP matrix in the blends. Deformation of a semi-crystalline polymer can be viewed as the stretch of amorphous network with crystallites as physical cross-links[29]. The network-like crystalline textures of C10 and C30 not only strengthen the toughness but also keep the strength[30], which is consistent with the results of the mechanical properties testing. However, morphology image of *co*-PP is obviously different from that of pure *i*PP and the blends, and the size of spherulites is too small to be seen, as exhibited in Figs. 6(c), 7(d) and 7(d′). This may be caused by the compositions and structures of *co*-PP.

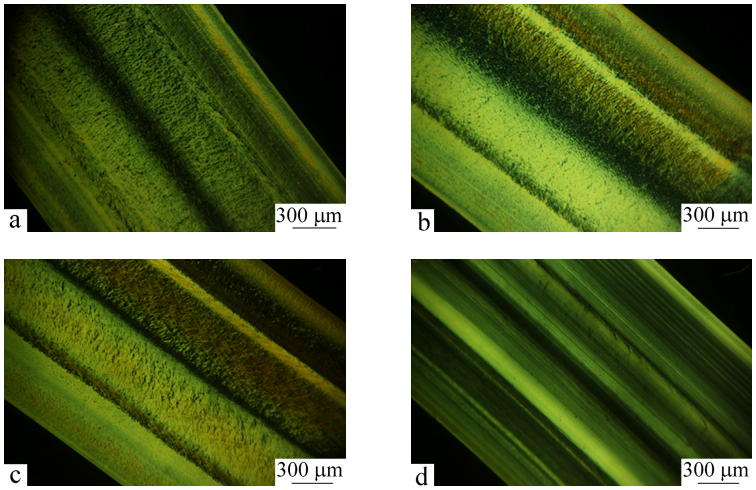
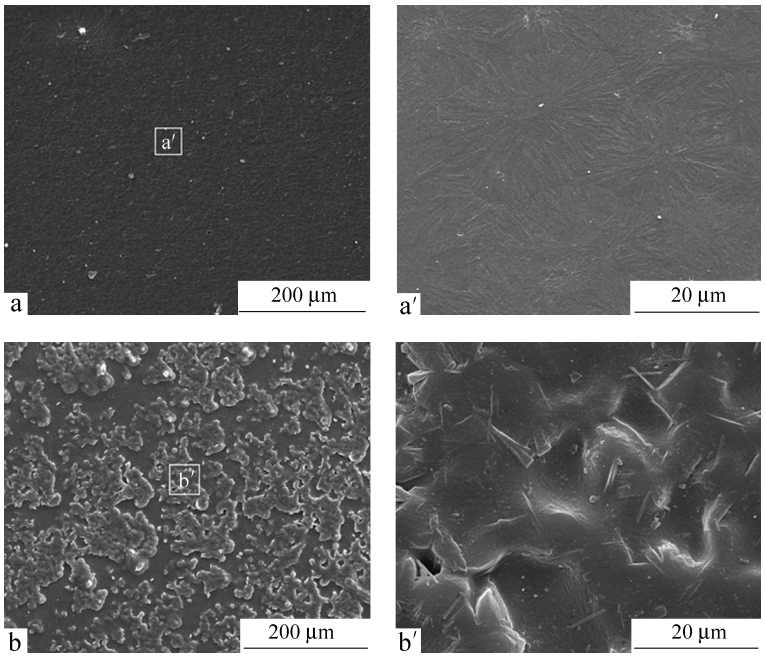



**Fig. 6** The POM images reflecting the morphology of the injection molded samples: (a) *i*PP, (b) C10, (c) C30 and (d) *co*-PP



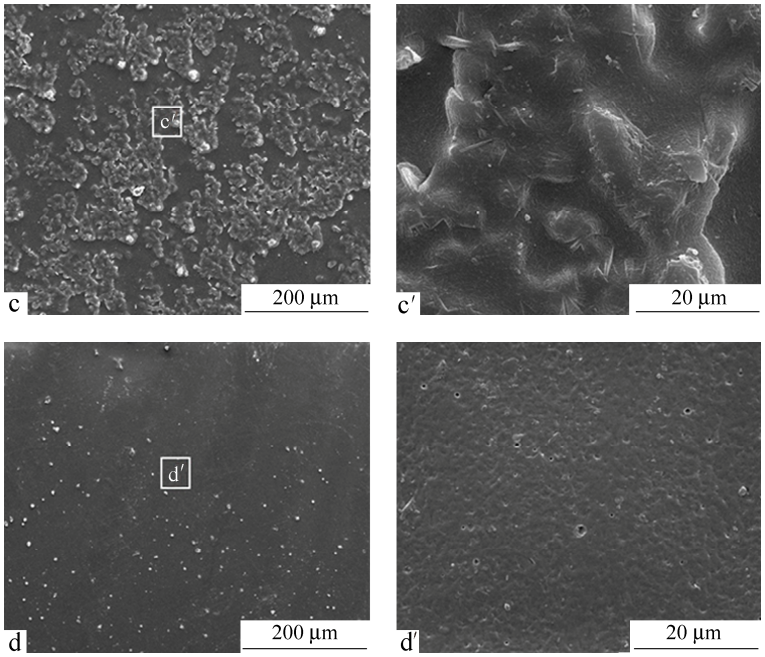



**Fig. 7** SEM images reflecting the morphology of the injection molded samples perpendicular to the flow direction: (a) *i*PP, (b) C10, (c) C30 and (d) *co*-PP
The images (a′), (b′), (c′) and (d′) correspond to the parts in the white boxes of the images (a), (b), (c) and (d), respectively.

Figure 8 shows evolution of morphology and crystalline structure of *i*PP/*co*-PP blends and the influence of *co*-PP on the crystallization of *i*PP with the help of variable-temperature POM. The crystallization starting temperature for C10 is much higher than that for pure *i*PP, which is in accordance with the DSC results. As shown in the images taken at 125 °C, there is almost no sign of crystal growth at 140 °C, while in C10 numerous

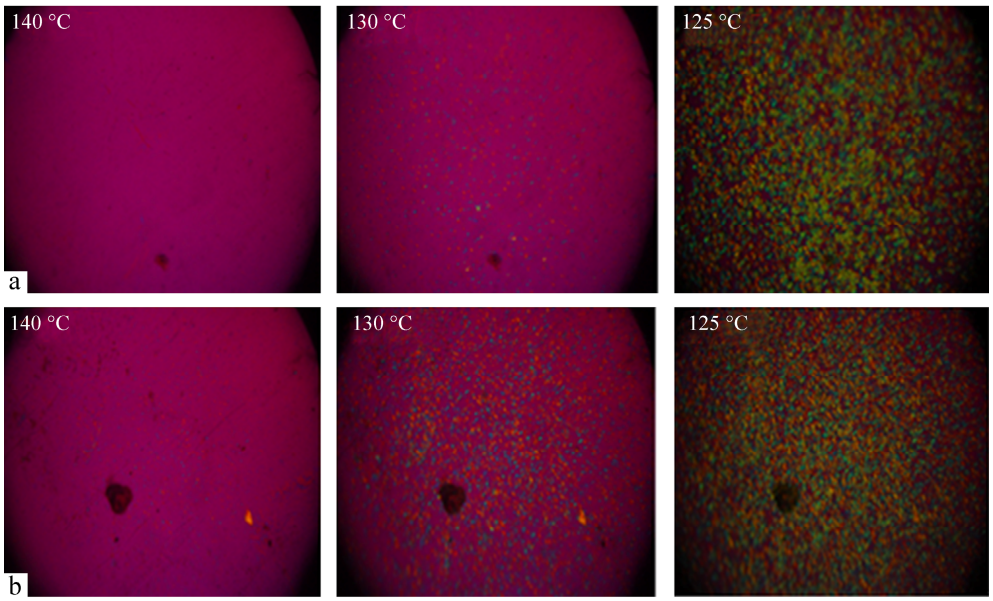



**Fig. 8** The POM images comparing the morphology evolution of pure *i*PP and C10 at 140 °C, 130 °C and 125 °C: (a) pure *i*PP and (b) C10

crystals are generated. When the temperature decreases to 130 °C, the crystalline growth rate of C10 is faster than that of pure *i*PP. The final crystal size of C10 is smaller than that of pure *i*PP, which can be clearly seen in the pictures taken at 125°C. The higher crystallization starting temperature, faster crystalline growth rate and smaller crystal size of C10 sample may be caused by the incorporation of small content of *co*-PP. This consequence is in accordance with the previous results.

***Mechanism***

Figure 9 illustrates the morphological evolution process of *i*PP, C10, C30 and *co*-PP samples. *i*PP with high degree of isotacticity (≥ 95%) will produce relatively large-sized $\alpha$-spherulites[31] during crystallization, which have structural integrity and clear-cut interface. When impacted, *i*PP will produce stress concentration easily in its crystalline region. Because the stress fields, which are unfavorable for energy transmission, are independent, so brittle fracture happened. Due to the compositions and structures of *co*-PP, small number of tiny crystals is formed during the crystallization.

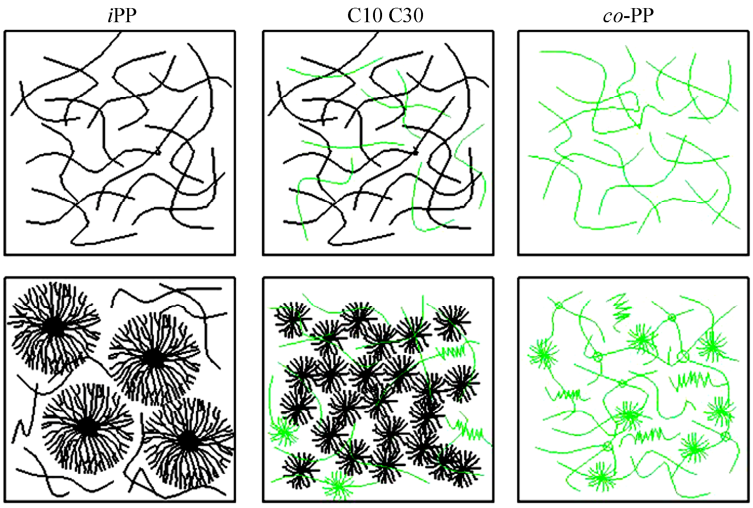



**Fig. 9** Schematic illustration of the morphology evolution of *i*PP, C10, C30 and *co*-PP during injection molding

For the C10 and C30, the incorporation of *co*-PP, which act as polymeric nucleating agents in the blends[32–36], substantially reduced the crystal size of *i*PP matrix, producing numerous and well-distributed tiny $\alpha$-spherulites. Due to the well compatibility of *co*-PP and *i*PP, *co*-PP molecular chains could penetrate *i*PP spherulites and then generate network-like crystalline structures. The network-like crystalline structure can transfer stress effectively, the impact fracture of *i*PP/*co*-PP blends is quasi ductile fracture dominated by multiple crazes with good toughness. The interaction between *co*-PP molecular chains and *i*PP crystalline regions will require more energy to overcome intermolecular forces in the process of stretching. Therefore, the strength of the material has been enhanced to some extent.

## CONCLUSIONS

The thesis conducted in-depth research into the crystallization behavior, rheological behavior, mechanical properties and microstructures of *i*PP, *co*-PP and *i*PP/*co*-PP blends. It discovered that *co*-PP and *i*PP are compatible with each other and the molecular chain segments of *co*-PP can entangle with those of *i*PP. The addition of small content of *co*-PP greatly reduced the crystalline size of *i*PP matrix in *i*PP/*co*-PP blends (C10, C30) and generated many evenly distributed tiny close-knit arranged $\alpha$-spherulites. The molecular chain segments of *co*-PP crossed *i*PP spherulites and formed network-like crystalline structure during crystallization. The network-like crystalline structure could transmit stress effectively, and the impact fracture mechanism of *i*PP/*co*-PP blends was quasi ductile fracture dominated by multiple crazes with good toughness. The penetration

of *co*-PP molecular chains into *i*PP crystalline region facilitated the intermolecular forces, which demanded more energy to overcome intermolecular forces to resist stretching. So the strength some extent improved. *co*-PP modified *i*PP materials with advanced toughness and strength were thus completely realized in C10 and C30.

## REFERENCES


1 Fu, Z.S., Fan, Z.Q., Zhang, Y.Q. and Feng, L.X., Eur. Polym. J., 2003, 39(4): 795
2 Zhang, Y., Liu, H., Zhang, L., Li, X.P., Du, H.N. and Zhang, J., J. Appl. Polym. Sci., 2013, 129(5): 2744
3 Zhang, Y., Zhang, L., Liu, H., Du, H.N., Zhang, J., Wang, T. and Zhang, X.W., Polymer, 2013, 54(21): 6026
4 Naiki, M., Matsumura, T. and Matsuda, M., J. Appl. Polym. Sci., 2002, 83(1): 46
5 Bassani, A. and Pessan, L.A., J. Appl. Polym. Sci., 2003, 88(4): 1081
6 Kamfjord, T. and Stori, A., Polymer, 2001, 42(7): 2767
7 Xu, J.T., Ding, P.J., Fu, Z.S. and Fan, Z.Q., Polym. Int., 2004, 53(9): 1314
8 Tan, H.S., Li, L., Chen, Z.N., Song, Y.H. and Zheng, Q., Polymer, 2005, 46(10): 3522
9 Chen, H.B., Karger-Kocsis, J., Wu, J.S. and Varga, J., Polymer, 2002, 43(24): 6505
10 Tanem, B.S., Kamfjord, T., Augestad, M., Lovgren, T.B. and Lundquist, M., Polymer, 2003, 44(15): 4283
11 Li, H., Zhang, X., Kuang, X., Wang, J., Wang, D., Li, L. and Yan, S., Macromolecules, 2004, 37(8): 2847
12 Sun, X., Li, H., Wang, J. and Yan, S., Macromolecules, 2006, 39(25): 8720
13 Dubnikova, I.L., Berezina, S.M. and Antonov, A.V., J. Appl. Polym. Sci., 2004, 94(5): 1917
14 Liang, J.Z. and Li, R.K.Y., J. Appl. Polym. Sci., 2000, 77(2): 409
15 Svoboda, P., Zeng, C.C., Wang, H., Lee, L.J. and Tomasko, D.L., J. Appl. Polym. Sci., 2002, 85(7): 1562
16 Olley, R.H. and Bassett, D.C., Polymer, 1982, 23(12): 1707
17 Zhang, X.D. and Shi, G.Y., Polymer, 1994, 35(23): 5067
18 Auriemma, F. and De, Rosa. C., Macromolecules, 2006, 39(22): 7635
19 Alamo, R.G., Ghosal, A., Chatterjee, J. and Thompson, K.L., Polymer, 2005, 46(20): 8774
20 Gou, Q., Li, H., Yu, Z., Chen, E., Zhang, Y. and Yan, S., Colloid. Polym. Sci., 2007, 285(10): 1149
21 An, Y., Gu, L., Wang, Y., Li, Y.M., Yang, W., Xie, B.H. and Yang, M.B., Mater. Des., 2012, 35: 633
22 Liu, K.J., Zhang, L., Liu, H., Deng, P., Du, H.N., Li, X.P. and Zhang, J., Mater. Lett., 2013, 90: 145
23 Jones, A.T., Aizlewood, J.M. and Beckett, D.R., Makromolekulare Chemie, 1964, 75: 134
24 Chen, Y., Chen, Y., Chen, W. and Yang, D., Polymer, 2006, 47(19): 6808
25 Kakugo, M., Miyatake, T., Mizunuma, K. and Kawai, Y., Macromolecules, 1988, 21(8): 2309
26 Hayashi, T., Inoue, Y., Chujo, R. and Asakura, T., Macromolecules, 1988, 21(9): 2675
27 Zhang, C.H., Shangguan, Y., Chen, R.F., Wu, Y.Z., Chen, F., Zheng, Q. and Hu, G., Polymer, 2010, 51(21): 4969
28 McKenna, T.F., Bouzid, D., Matsunami, S. and Sugano, T., Polym. React. Eng., 2003, 11(2): 177
29 Luo, F., Wang, J., Bai, H., Wang, K., Deng, H., Zhang, Q., Chen, F., Fu, Q. and Na, B., Mater. Sci. Eng. A-Struct., Mater. Proper. Microstruct. Proc., 2011, 528(22–23): 7052
30 Bai, H., Wang, Y., Zhang, D., Xiao, C., Song, B., Li, Y. and Han, L., Mater. Sci. Eng., A-Struct. Mater. Proper. Microstruct. Proc., 2009, 513–14: 22
31 Su, R., Li, Z., Bai, H., Wang, K., Zhang, Q., Fu, Q., Zhang, Z. and Men, Y., Polymer, 2011, 52(16): 3655
32 Su, Z., Wang, H., Dong, J., Zhang, X., Dong, X., Zhao, Y., Yu, J., Han, C.C., Xu, D. and Wang, D., Polymer, 2007, 48(3): 870
33 Su, Z., Dong, M., Guo, Z. and Yu, J., Macromolecules, 2007, 40(12): 4217
34 Su, Z.Q., Chen, X.N., Yu, Z.Z. and Zhang, L., J. Appl. Polym. Sci., 2009, 111(2): 786
35 Cao, L., Dong, M., Zhang, A., Liu, Y., Yang, W., Su, Z. and Chen, X., Polym. Eng. Sci., 2013, 53(12): 2674
36 Li, Q., Zhang, X.Y., Li, J.F., Ouyang, Z.F., Wang, H.X., Wei, G. and Su, Z.Q., Polym. Eng. Sci., 2014, 54(9): 2112